HHS Public Access

Author manuscript

Oncogene. Author manuscript; available in PMC 2024 August 01.

Published in final edited form as:

Oncogene. 2023 August ; 42(35): 2629–2640. doi:10.1038/s41388-023-02792-6.

Activation of NFAT by HGF and IGF-1 via ARF6 and its effector ASAP1 promotes uveal melanoma metastasis

Jackson R. Richards[1,2,12], **Donghan Shin**[2], **Rob Pryor**[2], **Lise K. Sorensen**[2], **Zhonglou Sun**[2], **Won Mi So**[3], **Garam Park**[3], **Roger Wolff**[4,5], **Amanda Truong**[1,5], **Martin McMahon**[1,5,6], **Allie H. Grossmann**[4,5,7], **J. William Harbour**[8], **Weiquan Zhu**[2,9], **Shannon J. Odelberg**[2,9,10,*], **Jae Hyuk Yoo**[3,11,*]

[1]Department of Oncological Sciences, School of Medicine, University of Utah, 2000 Circle of Hope Drive, Salt Lake City, UT 84112, USA,

[2]Department of Medicine, Program in Molecular Medicine, University of Utah, 15 North 2030 East, Salt Lake City, UT 84112, USA

[3]Department of Ophthalmology & Visual Sciences, Truhlsen Eye Institute, University of Nebraska Medical Center, Omaha, NE 68198, USA

[4]Department of Pathology, University of Utah, 15 North Medical Drive East, Salt Lake City, UT 84112, USA

[5]Huntsman Cancer Institute, University of Utah Health Sciences Center, 2000 Circle of Hope Drive, Salt Lake City, UT 84112, USA

[6]Department of Dermatology, University of Utah, 30 N 1900 E, Salt Lake City, UT 84132, USA

[7]ARUP Laboratories, University of Utah, 500 Chipeta Way, Salt Lake City, UT 84112, USA

[8]Department of Ophthalmology, Harold C. Simmons Comprehensive Cancer Center, UT Southwestern Medical Center, Dallas, TX, 75390, USA

[9]Division of Cardiovascular Medicine, Department of Medicine, University of Utah, 30 North 1900 East, Salt Lake City, UT 84132, USA

[10]Department of Neurobiology and Anatomy, University of Utah, 20 South 2030 East, Salt Lake City, UT 84112, USA

[11]Fred and Pamela Buffett Cancer Center, University of Nebraska Medical Center, Omaha, NE 68198, USA

[*]Corresponding Authors: Shannon J. Odelberg, Building 533 Room 4110B, 15 North 2030 East, Salt Lake City, UT 84112, USA, sodelber@genetics.utah.edu; Jae Hyuk Yoo, BCC, 7.12.318, 505 S 45th St., Omaha, NE 68198-6837, USA, jyoo@unmc.edu.
These authors contributed equally as corresponding authors

AUTHOR CONTRIBUTIONS

SJO and JHY were responsible for conceptualization, experimental design, data analysis, and manuscript preparation. JHY primarily performed and collected data for *in vitro* experiments. JRR and DS primarily performed and collected data for *in vivo* experiments. RP, ZS, WMS, GP, and AT performed *in vitro/in vivo* experiments. LKS performed immunocytofluorescent staining. RW performed bioinformatic analyses. AHG provided histology and pathology expertise. MM, AHG, JWH, and WZ provided resources and critical review of the manuscript. All authors read the manuscript, agree with the content, and were given the opportunity to provide input.

COMPETING INTERESTS

J.W.H. is the inventor of intellectual property related to prognostic testing in uveal melanoma. He is a paid consultant for Castle Biosciences, licensee of this intellectual property, and he receives royalties from its commercialization.

[12]Current Address: Department of Psychiatry, Carver College of Medicine, University of Iowa, Iowa City, IA 52242, USA

Abstract

Preventing or effectively treating metastatic uveal melanoma (UM) is critical because it occurs in about half of patients and confers a very poor prognosis. There is emerging evidence that hepatocyte growth factor (HGF) and insulin-like growth factor 1 (IGF-1) promote metastasis and contribute to the striking metastatic hepatotropism observed in UM metastasis. However, the molecular mechanisms by which HGF and IGF-1 promote UM liver metastasis have not been elucidated. *ASAP1*, which acts as an effector for the small GTPase ARF6, is highly expressed in the subset of uveal melanomas most likely to metastasize. Here, we found that HGF and IGF-1 hyperactivate ARF6, leading to its interaction with ASAP1, which then acts as an effector to induce nuclear localization and transcriptional activity of NFAT1. Inhibition of any component of this pathway impairs cellular invasiveness. Additionally, knocking down *ASAP1* or inhibiting NFAT signaling reduces metastasis in a xenograft mouse model of UM. The discovery of this signaling pathway represents not only an advancement in our understanding of the biology of uveal melanoma metastasis but also identifies a novel pathway that could be targeted to treat or prevent metastatic uveal melanoma.

INTRODUCTION

Uveal melanoma arises from transformed melanocytes of the uveal tract, most often in the choroid [1]. The primary tumor can be effectively managed with radiation therapy and, when necessary, enucleation [2]. Despite this, approximately half of patients develop metastatic disease, usually several years after their primary tumors are treated [3, 4]. Outcomes for these patients are dismal; median survival is less than one year [5]. The liver is the predominant site of uveal melanoma metastasis, and liver-directed therapies increase median overall survival [5, 6]. However, long-term remission of metastatic uveal melanoma has very rarely been achieved [7–10]. There is thus a pressing need to better understand the biology of metastatic uveal melanoma and to develop therapies to treat and, if possible, prevent this stage of disease.

Evidence suggests that driver mutations occur early in the development of a particular uveal melanoma and have little influence on the risk of metastasis [11, 12]. Other molecular alterations, however, along with stage and histologic features, have significant prognostic implications [13]. Metastatic risk groups have been generated by analysis of mutations, gene expression, and other molecular markers [14–18]. However, these alterations alone do not explain the hepatotropism of metastatic uveal melanoma. Recent work suggests that growth factors generated in the liver, such as hepatocyte growth factor (HGF) and insulin-like growth factor 1 (IGF-1), may contribute to this phenomenon [19–22].

Previously, we demonstrated that the small GTPase ARF6 contributes to tumorigenesis of uveal melanoma by controlling the trafficking and thereby oncogenic signaling of GNAQ [23]. In numerous other cancers, ARF6 has been implicated in the processes of invasion and metastasis, rather than tumorigenesis [24, 25]. In many such cases, ARF6 is

activated by receptor tyrosine kinases (RTKs), including c-MET, the cognate receptor of HGF [24, 26, 27]. We therefore asked whether growth factors such as HGF and IGF-1 might hyperactivate ARF6 and contribute to invasion and metastasis in uveal melanoma via divergent pathways from GNAQ signaling. We hypothesized that ASAP1 (ArfGAP with SH3 domain, ankyrin repeat, and PH domain 1; also known as AMAP1 and DDEF1), which is a GTPase activating protein for ARF1 [28] but an effector for ARF6 [29], might play a role in signaling pathways mediating invasion and metastasis. *ASAP1* is located on 8q, the amplification of which is associated with uveal melanoma metastasis in a dose-dependent manner [14, 30]. Additionally, in an analysis comparing primary uveal melanoma tumors with 8q amplification to those without, *ASAP1* was the most overexpressed of genes on 8q [31]. By contrast, the expression of *MYC*, a well-known oncogene in other cancers, was not increased in tumors with increased copy numbers of 8q. Furthermore, in this same study, overexpression of *ASAP1* in low-grade uveal melanoma cells induced migration *in vitro* [31]. However, no previous *in vivo* evidence has been generated demonstrating a direct mechanistic link between ASAP1 and uveal melanoma metastasis.

Here, we report that both HGF and IGF-1 enhance uveal melanoma cell invasion by hyperactivating ARF6, which then acts through ASAP1 to activate NFAT1 via a calcineurin-dependent mechanism. Inhibiting this pathway by knockdown of *ASAP1* or inhibition of NFAT significantly reduces metastatic disease in a xenograft model of human uveal melanoma.

RESULTS

Hepatocyte growth factor (HGF) and insulin-like growth factor-1 (IGF-1) hyper-activate ARF6 and promote invasion of uveal melanoma

Given that activated ARF6 promotes invasion and metastasis of many human cancers [24, 32], we first tested whether ARF6 is activated by growth factors that may contribute to hepatic tropism, such as HGF and IGF-1. We treated OMM1 and OMM2.5 cells (Supplementary Table 1) with HGF or IGF-1 and assessed ARF6-GTP levels. Both cell lines showed a time-dependent increase in ARF6 activation upon stimulation with either growth factor (Fig. 1A). Next, we asked whether this activation is required for cellular invasion of uveal melanoma. When performing invasion assays, we pretreated uveal melanoma cells with 10 μg/mL Mitomycin C to ensure that they would not proliferate during the invasion assay (Supplementary Fig. 1A) [33]. Using Matrigel invasion assays, we determined that HGF and IGF-1 significantly increased invasion of both cell lines when they were transduced with a control (null) adenovirus. By contrast, when the cells were transduced with $ARF6^{T27N}$, a dominant-negative form of ARF6, their invasiveness was significantly reduced (Fig. 1B). Consistent with these results, knockdown of *ARF6* with siRNA likewise reduced Matrigel invasion of HGF- and IGF-1-stimulated OMM2.5 cells (Fig. 1C, Supplementary Fig. 1B), and ARF6 inhibition by ectopic $ARF6^{T27N}$ expression reduced invasion through a collagen matrix (Fig. 1D). Additionally, constitutively active $ARF6^{Q67L}$ increased the invasiveness of OMM1 and OMM2.5 cells (Fig. 1E). Based on gene expression profiles, uveal melanomas can be classified as either class I or class II, with class II exhibiting greater metastatic potential [34]. Using a limited number of tumors,

we observed a trend towards increased ARF6-GTP levels in class II human primary uveal melanoma tumors (Supplementary Fig. 1C, D). Collectively, these results indicate that hyperactivation of ARF6 by HGF and IGF-1 promotes invasion of uveal melanoma cells.

ASAP1 is required for invasion and metastasis of uveal melanoma

To determine how ARF6 might control uveal melanoma cell invasion, we investigated whether the expression of ARF6 and its effector ASAP1 were associated with clinical outcomes in patients with uveal melanoma. Using the Cancer Genome Atlas Uveal Melanoma (TCGA UVM) RNA sequencing dataset, we found that high expression of either ARF6 or ASAP1 is significantly associated with both decreased time to metastasis and decreased survival rates (Fig. 2A–D).

We then asked whether ASAP1 is required for cellular invasion of uveal melanoma stimulated by activated ARF6. Knocking down *ASAP1* expression with siRNA following the hyperactivation of ARF6, either by ectopic expression of constitutively active $ARF6^{Q67L}$ or by treatment with HGF or IGF-1, significantly reduced invasion of uveal melanoma cells through Matrigel in three uveal melanoma cell lines, OMM1, OMM2.5, and MP38 (which exhibits loss of BAP1) (Fig. 2E–2G, Supplementary Fig. 2A, B; Supplementary Table 1).

We next determined the effects of *ASAP1* knockdown on metastatic behavior in a mouse xenograft model of uveal melanoma. Luciferase-expressing OMM2.5 cells were injected into the retro-orbital sinus, and metastasis in trunk organs was monitored using bioluminescence imaging. Quantification of trunk bioluminescence flux revealed that metastatic burden was significantly reduced in mice that received cells expressing *ASAP1* shRNA compared to those expressing control shRNA (Fig. 2H; mixed effects model $p<0.0001$). The incidence of metastasis was also reduced in the *ASAP1* knockdown group (Fig. 2I). Representative bioluminescence images at week six are shown in Figure 2J. Histologic examination of livers and lungs corroborated the bioluminescence data (Fig. 2K), indicating that blocking ASAP1 function inhibits metastasis to both organs. Together, these results strongly suggest a significant role for ASAP1 in uveal melanoma invasion and metastasis.

In other cancer cells, ASAP1 has been suggested to be an effector, rather than GTPase activating protein (GAP), of ARF6 because it selectively binds ARF6-GTP yet does not stimulate GTP hydrolysis [35]. We therefore asked whether activated ARF6 interacts with ASAP1 in uveal melanoma cells. We incubated the recombinant glutathione-S-transferase (GST)-tagged GAP domain of ASAP1 with lysates from OMM2.5 cells that had been transduced with an adenovirus expressing either dominant-negative $ARF6^{T27N}$ or constitutively active $ARF6^{Q67L}$. GST pulldown and immunoblotting revealed that $ARF6^{Q67L}$ physically interacts with the ASAP1 GAP domain but $ARF6^{T27N}$ does not (Supplementary Fig. 2C). Additionally, either transient or stable knockdown of *ASAP1* decreased invasiveness of OMM1 and OMM2.5 cells as measured by Matrigel invasion assays (Supplementary Fig. 2D, E). From these results, we conclude that ASAP1 forms a complex with activated ARF6 and acts as an effector to promote uveal melanoma cell invasion.

Activated ARF6 increases NFAT1 nuclear localization and transcriptional activity

We next sought to determine the mechanism by which ARF6-ASAP1 signaling controls the invasiveness of uveal melanoma cells. Although it has been shown that ARF6-ASAP1 mediates changes in the cytoskeleton architecture of tumor cells that promote breast cancer metastasis [29], it is not known whether ARF6-ASAP1 activates tumor-associated transcription factors that induce metastasis. Our previous work showed that ARF6 acted downstream of mutant Gαq to promote oncogenic pathways that induced transcription [23]. Therefore, we took a broader approach and used an array containing 96 transcription factors to identify those that are increased in the nuclei of cells ectopically expressing $ARF6^{Q67L}$. The NFAT family of transcription factors [36] was among the most highly upregulated (Supplementary Table 2) when compared to cells expressing a control (null) adenovirus. We therefore examined protein levels of different NFAT isoforms in cells expressing $ARF6^{Q67L}$. Only NFAT1 was expressed in both OMM1 and OMM2.5 cell lines and exhibited increased expression levels in response to ectopic expression of $ARF6^{Q67L}$ (Supplementary Fig. 3A, B).

We then investigated the effects of $ARF6^{Q67L}$ on the localization and transcriptional output of NFAT1. Subcellular fractionation revealed that ARF6 activation significantly increased nuclear localization of NFAT1, while cytoplasmic levels appeared to be increased as well (Fig. 3A, B). Visualization of NFAT1 by immunocytofluorescence in OMM2.5 cells corroborated this finding (Fig. 3C). Lastly, utilizing a luciferase reporter for NFAT, we found that $ARF6^{Q67L}$ significantly increases NFAT transcriptional activity in both cell lines (Fig. 3D). Consistent with these *in vitro* cellular results, we found that increased *NFATC2* (the gene encoding NFAT1) expression is associated with decreased time to metastasis and reduced survival rates in patients included in the UVM TCGA database (Fig. 3E, F). Together, these results demonstrate that ARF6 activation increases nuclear localization and transcriptional activity of NFAT1 and suggest that this pathway may contribute to uveal melanoma metastasis.

ARF6 and ASAP1 are required for nuclear localization and transcriptional activity of NFAT1 induced by HGF and IGF-1

Given our unexpected finding that $ARF6^{Q67L}$ induces NFAT1 nuclear translocation and transcriptional activity, we asked whether HGF- and IGF-1-induced ARF6 activation also increases NFAT1 activity. Using subcellular fractionation of OMM2.5 lysates, we first found that IGF-1, HGF, or the combination of both factors increased both total and nuclear NFAT1. Conversely, the expression of dominant-negative $ARF6^{T27N}$ significantly reduced baseline levels and transcriptional activity of nuclear NFAT1 and attenuated NFAT1 induction by these growth factors (Fig. 4A–C, Supplementary Fig. 4A–C). Corollary experiments in which cells were transfected with control or *ASAP1* siRNA and then treated with the combination of growth factors yielded similar results (Fig. 4D–F, Supplementary Fig. 4D–F), thus allowing us to conclude that both ARF6 and ASAP1 are necessary for HGF- and IGF-1-induced nuclear translocation of NFAT1 and its transcriptional activity in uveal melanoma cells.

ARF6, *ASAP1*, and *NFATC2* expression levels are correlated in uveal melanoma patients

Given that the expression levels of *ARF6*, *ASAP1*, and *NFATC2* were each associated with poor prognosis in uveal melanoma patients in the TCGA database, we explored whether the expression levels of these genes were correlated with each other and found a statistically significant correlation for each pairwise comparison using Pearson's correlation coefficient (Supplementary Figure 4G; *ARF6*/*ASAP1*, Corr: 0.515, $p < 0.001$; *ARF6*/*NATFC2*, Corr: 0.386, $p < 0.001$; *ASAP1*/*NFATC2*, Corr: 0,388, $p < 0.001$).

Calcineurin and NFAT inhibitors reduce HGF- and IGF-1-induced invasion

Calcineurin is a phosphatase that activates NFAT transcription factors by binding and dephosphorylating them at several key residues [37]. We employed three inhibitors of calcineurin-NFAT signaling to test whether pharmacologic inhibition reduces HGF- and IGF-1-induced invasion of uveal melanoma cells. Cyclosporin A and tacrolimus (also known as FK506) are molecules that bind immunophilin proteins and prevent calcineurin from accessing its substrates [37]. 11R-VIVIT is a small peptide that competitively inhibits NFAT from binding calcineurin without affecting its phosphatase activity; it is thus more selective than the calcineurin inhibitors [38, 39].

Using Matrigel invasion assays, we found that treatment (1 μM) with either of the calcineurin inhibitors completely abrogated invasion induced by HGF or IGF-1 in OMM1 and OMM2.5 cells (Fig. 5A). Treatment with 11R-VIVIT (1 μM) produced the same response in both cell lines as well as in the BAP1 mutant cell line MP38 (Fig. 5B), while 11R-VIVIT reduced baseline invasion significantly in the OMM1 cell line (Fig. 5B). *NFATC2* knockdown in HGF- and IGF-1-stimulated OMM2.5 cells also inhibited Matrigel invasion (Fig. 5C), while 11R-VIVIT inhibited growth factor-treated OMM2.5 cells through a collagen matrix (Fig. 5D). We also assessed the effects of these inhibitors on cellular proliferation. Interestingly, cyclosporin A and tacrolimus inhibited proliferation in a dose-dependent manner (Supplementary Fig. 5A, B). By contrast, concentrations up to 5 μM of 11R-VIVIT did not significantly affect proliferation of OMM2.5 cells and only slightly reduced proliferation of OMM1 cells (Supplementary Fig. 5C). These results suggest that NFAT signaling is required for invasion while calcineurin activity, which regulates other downstream proteins in addition to NFAT, is necessary for both invasion and proliferation of uveal melanoma cells.

Inhibiting NFAT reduces uveal melanoma metastasis

Given our finding that inhibition of calcineurin-NFAT signaling potently reduced invasion of uveal melanoma cells, we asked whether it would also reduce metastasis *in vivo*. To test this, we generated stable OMM2.5 cell lines that ectopically express EGFP alone or VIVIT (the small peptide inhibitor of NFAT) fused to EGFP. We first characterized the effects of EGFP-VIVIT expression on NFAT1 localization and cellular phenotypes *in vitro*. Compared to EGFP alone, expression of EGFP-VIVIT reduced nuclear accumulation of NFAT1 and transcriptional activity in an NFAT luciferase reporter assay in response to treatment with HGF and IGF-1 (Fig. 6A, B, Supplementary Fig. 6A). Furthermore, these cells were less invasive, as evidenced by the abrogation of invasiveness when exposed to these growth factors (Fig. 6C).

We next tested the metastatic capacity of these cells using the retro-orbital injection model. Mice that received injections of OMM2.5 EGFP-VIVIT cells exhibited reduced trunk tumor burden by approximately 3.9-fold eight weeks after retro-orbital injection as measured by bioluminescence imaging (Fig. 6D; mixed effects model $p<0.0001$). The incidence of metastasis was also reduced in mice that were injected with cells expressing EGFP-VIVIT (Fig. 6E). Representative bioluminescence images of mouse trunks at week eight are shown in Figure 6F. Histopathological evaluation of liver metastases was consistent with the bioluminescence data (Fig. 6G).

We next investigated whether pharmacological inhibition of calcineurin affects uveal melanoma metastasis in a mouse xenograft model of uveal melanoma. Systemic treatment by oral gavage of the calcineurin inhibitor tacrolimus also reduced uveal melanoma metastastic burden in a mouse xenograft model of uveal melanoma by approximately 4.2-fold twelve weeks after retro-orbital injection (Supplementary Fig. 6B, C). These results suggest that inhibition of NFAT might be a new therapeutic option for patients with metastatic uveal melanoma.

DISCUSSION

The molecular mechanisms underlying metastasis of uveal melanoma are poorly defined. A more thorough understanding of this process might lead to new treatments and better outcomes for patients with this deadly cancer. In this study, using cellular and biochemical methods, as well as mouse models, we identify a novel signaling pathway that is required for efficient invasion and metastasis of uveal melanoma. HGF and IGF-1 hyperactivate ARF6, which physically interacts with the GAP domain of ASAP1. In this context, ASAP1 acts as an ARF6 effector and increases protein levels, nuclear translocation, and transcriptional activity of NFAT1. Loss of ASAP1 or inhibition of NFAT impairs invasion of uveal melanoma cells and metastasis *in vivo* (Fig. 6H).

The findings reported in this study provide direct *in vivo* evidence of a role for ASAP1 in uveal melanoma metastasis and help elucidate the molecular mechanisms by which ASAP1 functions to promote metastasis. Previous studies in other cancers have suggested that ASAP1 may function as an ARF6 effector to induce the formation of invadopodia by interacting with cortactin, paxillin, possibly Amp II, and indirectly with integrins [29]. Here, we show that ASAP1 can act as an ARF6 effector to induce the activation of the transcription factor NFAT1, which promotes uveal melanoma cell invasion and metastasis. Thus, our work suggests a new functional role for ASAP1 in controlling metastasis. Whether ASAP1 also activates other transcription factors involved in uveal metastasis remains to be determined. As a first step in the process, we identified several other transcription factors that are activated by the ectopic expression of $ARF6^{Q67L}$ in uveal melanoma cells (Supplementary Table 2). These might also be regulated by the ARF6-GTP–ASAP1 complex, and future studies should determine whether they also play a role in invasion and metastasis.

Although it is the activation of the HGF/IGF-1–ARF6–ASAP1–NFAT1 pathway that drives uveal melanoma metastasis rather than the expression levels of the individual components

of the pathway, high expression levels could enhance signaling. Therefore, it is interesting to note that high expression levels of *ARF6*, *ASAP1*, and *NFATC2* are each correlated with worse prognosis in patients. In this context, it is also noteworthy that there is a statistically significant positive correlation in gene expression levels between these three essential components of the pathway, although the correlations are not extremely strong (Pearson's Correlation coefficients: 0.386–0.515) (Supplementary Fig. 4G).

Approximately half of all uveal melanoma patients will develop metastatic disease and in about 93% of these patients, metastasis will be found in the liver with 57% of these cases exclusively exhibiting liver metastasis [40]. Lung metastasis occurs in about 24% of patients who experience metastasis [40]. In one study using our retro-orbital model, we observed gross liver metastasis in 14 out of 24 mice that exhibited trunk bioluminescence. Given that our focus was on liver metastasis and hepatotropism, we did not examine the lung in all mice and therefore do not have comparable data for lung metastasis, although it was readily observed in some mice (Fig. 2K). These results suggest that our model produces liver metastasis in most mice that exhibit trunk metastasis, although an accurate percentage cannot be determined from these data because we did not histologically examine entire livers to detect cryptic or micro metastases.

In our retro-orbital injection model, the initial steps of tumor cell egress from the primary tumor and intravasation into blood vessels are bypassed. We are therefore testing the ability of the tumor cells to survive in the bloodstream, arrest in a distant organ, extravasate and invade into a new tissue, and grow as a metastatic nodule [41]. We hypothesize that ARF6-ASAP1-NFAT1 signaling is crucial for tumor cell motility during the processes of extravasation and migration in the early stages of metastatic colonization. Perhaps these processes are most stimulated in areas with high concentrations of HGF and IGF-1, possibly explaining the tropism for the liver. Therapeutically targeting this pathway in the adjuvant setting might reduce the formation of metastases and significantly improve outcomes for patients with uveal melanoma [42].

We recognize that pharmacologically targeting tumor NFAT signaling would have the clinically undesirable effect of systemic immunosuppression. Studying this is not feasible in xenograft mouse models because the mice are already genetically immunosuppressed. The effectors of NFAT signaling in uveal melanoma cells might therefore be more attractive therapeutic targets. Several proteins induced by NFAT have been implicated in the progression of numerous cancer types, including cutaneous melanoma [43, 44]. Additionally, a previous study performed integrated pathway analysis on patient tumors and discovered that increased activation of the NFATC2 (NFAT1 protein) pathway is associated with TCGA class 4 uveal melanoma, the group with the highest risk of metastasis [14]. Because NFAT proteins are known to interact with a diverse set of transcription factors [45], identifying target genes responsible for the observed phenotype using an unbiased approach might identify proteins and pathways that mediate invasion and metastasis of uveal melanoma.

Our previous work demonstrated the importance of ARF6 activation in $GNAQ^{Q209L}$-mediated oncogenic signaling and tumor growth [23]. Here, we expand this work and

show that HGF and IGF-1, factors thought to contribute to the hepatotropism of metastatic uveal melanoma [19–22], can induce hyperactivation of ARF6 and promote its interaction with ASAP1, leading to the activation of NFAT1 and increased uveal melanoma invasion and metastasis. Although ASAP1 also acts as an effector of activated ARF6 to promote oncogenic signaling and cell proliferation (Supplementary Fig. 7), the hyperactivation of ARF6 by HGF and IGF-1 appears to be important for uveal melanoma invasion and metastasis. Thus, ARF6 plays an active role in both the oncogenic and metastatic signaling pathways that control uveal melanoma and targeting the pathways controlled by ARF6 has the potential for treating both primary and metastatic uveal melanoma.

In summary, we describe a heretofore unknown signaling pathway in which growth factors produced in the liver activate the small GTPase ARF6, which acts through its effector ASAP1 to increase NFAT1 transcriptional output in uveal melanoma cells. This pathway is necessary for both invasion and metastasis and can be therapeutically targeted with inhibitors to reduce metastatic burden.

MATERIALS AND METHODS

Cell lines, Cytokines, and inhibitors

OMM1 cells were kindly shared by Kang Zhang (UCSD). All uveal melanoma cells were maintained in RPMI 1640 medium (ATCC) supplemented with 10% fetal bovine serum (Sigma-Aldrich) and 1% penicillin/streptomycin (Gibco). Cell line identity was confirmed by STR analysis (Promega) performed by the University of Utah DNA Sequencing Core.

Recombinant hepatocyte growth factor (HGF) and insulin-like growth factor 1 (IGF-1) were purchased from Peprotech. Cyclosporin A and tacrolimus (FK-506) were purchased from Selleckchem and dissolved in DMSO (ATCC). 11R-VIVIT [39], a peptide inhibitor of NFAT, was synthesized by Peptide 2.0.

Proliferation and Matrigel invasion assays

Cellular proliferation was assessed using the CyQUANT NF Cell Proliferation assay (Invitrogen) as previously described [23]. Transwell Matrigel invasion assays (Corning) and QCM Collagen cell invasion assays (Millipore) were used to assess cellular invasion. For Matrigel invasion assays, cells were treated with Mitomycin C (10 μg/mL) for two hours to inhibit proliferation and then seeded at a density of 50,000 – 200,000 uveal melanoma cells in 500 μL of RPMI with no FBS in upper chambers, while 500 μL of complete medium (RPMI + 10% FBS) was added to the lower chambers. FBS was replaced by HGF (50 ng/mL), IGF-1 (100 ng/mL), or both HGF and IGF-1 in the lower chamber when the effects of these growth factors were being tested. After 48 hours, cells that had migrated through the Matrigel were stained with Calcein AM dye (1 μg/mL) for one hour. Fluorescence (485 nm excitation and 530 nm emission) was then quantified using a plate reader (Bio-Tek Instruments). QCM Collagen cell invasion assays were performed according to the manufacturer's instructions.

ARF6 activation, immunoblotting, subcellular fractionation, and quantification

ARF6-GTP levels were assessed using the ARF6 Activation Assay Kit (Cell Biolabs). Before treatment, cells were grown in RPMI media without FBS for 48 hours. After treatment with HGF (50 ng/mL) or IGF-1 (100 ng/mL), cells were rinsed with ice-cold PBS, and dishes were frozen on dry ice. ARF6-GTP pulldowns were performed as previously described [46].

For immunoblotting, cells were lysed in ice-cold Pierce IP lysis buffer (25 mM HEPES, pH 7.4; 150 mM NaCl; 1% NP-40; 1 mM EDTA; 5% glycerol) with protease and phosphatase inhibitors (Halt™ cocktail; Thermo Fisher), centrifuged for 10 minutes at 14,000 rpm, and the supernatants were used to determine protein concentrations by BCA assays (Thermo Fisher). Each well of an SDS polyacrylamide gel was loaded with an equal amount of protein, and electrophoresis was conducted using Mini-PROTEAN Tetra cells (Bio-Rad). Separated proteins were transferred to PVDF membranes (Immobilon) using the Trans-Blot Turbo system (Bio-Rad). Primary antibodies (see Supplementary Table 3) were diluted in blocking buffer (either 5% non-fat dry milk or 5% BSA in phosphate- or Tris-buffered saline plus 0.1% Tween 20), and membranes were incubated on a shaker overnight at 4°C. After washing, secondary antibodies (see Supplementary Table 3) were applied at room temperature for one hour. Following another washing step, a chemiluminescent HRP substrate (Immobilon) was applied, and images were developed on Biomax MR film or ChemiDoc imaging system (Bio-Rad).

Cytosolic and nuclear fractionation was performed using NE-PER Nuclear and Cytoplasmic Extraction Reagents (Thermo Fisher) according to the manufacturer's instructions. Quantification for all immunoblots was performed by ImageJ. Signals were normalized to loading control, input, and/or total particular protein level, and the data displayed represent an amalgamation of all independent experimental replicates.

RNA interference, plasmids, transfections, adenoviral and lentiviral transduction

Control (Qiagen) and ASAP1 siRNA (Dharmacon) were used; further details and sequences are listed in Supplementary Table 4. Cells were transfected with siRNA duplexes in Lipofectamine RNAiMax (Invitrogen) and serum-free optiMEM with Glutamax (Gibco).

Lipofectamine LTX (Invitrogen) was used for plasmid transfection. An N-terminally HA-tagged human NFAT1 construct was cloned into pMEV-2HA (Biomyx) using pMIG-hNFATc2 [47] (Addgene plasmid #74050). For expression of EGFP or EGFP-VIVIT, cells were transfected with pEGFP-N1 [48] (Addgene plasmid #60360) or EGFP-VIVIT [38] (Addgene plasmid #11106). To generate stable lines, transfected cells were selected with Geneticin (800 μg/mL; Gibco) for two weeks.

Adenoviral constructs for Myc/His-ARF6^{Q67L}, Myc/His-ARF6^{T27N}, and Null (empty viral backbone) were designed in our lab [49] and purchased from Vector Biolabs.

Lentiviruses were used to generate stable cell lines for use in xenografts. Cells were at approximately 70% confluence and transduced with 1×10^6 PFU/mL. First, they were transduced with RFP-luciferase (amsbio) and selected using blasticidin (10 μg/mL:

InvivoGen). Cells then underwent a second transduction with lentivirus encoding for control or *ASAP1* shRNA (Sigma; see Supplementary Table 4) and selection with puromycin (1 μg/mL; InvivoGen) for two weeks.

Luciferase reporter assay

Uveal melanoma cells were transduced with an NFAT firefly luciferase reporter lentivirus (Cignal Lenti NFAT Reporter; Qiagen) and selected in puromycin (1 μg/mL; InvivoGen) for two weeks. Following treatment with siRNA or cytokines for each condition, 10 μg of cell lysate was assayed for luciferase activity using a Luciferase Assay System (Promega).

Immunocytofluorescence

Cells were seeded at a density of 10^5 cells/well in 8-well chambered coverglasses coated with fibronectin (10 μg/mL; Alfa Aesar). Cells were fixed for 20 minutes in 10% neutral buffered formalin and then washed three times in the buffer (PBS including 0.01% Ca^{2+}, 0.01% Mg^{2+}, and 0.1% sodium azide). Cells were permeabilized for 5 minutes in 0.1% Triton X-100 in the buffer. Wells were washed three times with the buffer and then blocked for 60 minutes at room temperature in 3% BSA diluted in the buffer. An antibody against NFAT1 (Cell Signaling Technology) was diluted 1:100 in the same blocking solution and applied to cells overnight at 4°C. The following day, cells were washed four times in the buffer, and 10 μg/mL Alexafluor 488-conjugated anti-Rabbit IgG (Thermo Fisher) diluted in blocking solution was applied in a dark box at room temperature for one hour. Wells were washed four times with the buffer, and DAPI anti-fade medium was added. Fields were randomly selected on the DAPI channel at 1,200 x with oil immersion. Z-stacked images (4 × 0.5 μm slices/field) were taken on an Olympus FV1000 confocal microscope.

Human uveal melanoma patient samples

These studies were done in accordance with a protocol approved by the University of Miami Institutional Review Board, and informed consent was obtained from all patients. Primary human uveal melanoma samples were collected and snap frozen at the time of enucleation by the J. William Harbour lab as previously described [50]. Tumors underwent pathologic evaluation, including classification as class I (low metastasis risk) or class II (high metastatic risk) by gene expression profiling [51]. De-identified samples were homogenized and lysed with ice-cold lysis buffer. Lysates were centrifuged for 20 minutes at 14,000 rpm and then used in ARF6-GTP pulldowns as described above.

Xenograft models of uveal melanoma, bioluminescence imaging, and quantification

Eight-week-old female NOD-Prkdc^{em26Cd52}Il2rg^{em26Cd22}/NjuCrl (NCG) mice were purchased from Charles River Laboratories. All animal experiments were approved by the Institutional Animal Care and Use Committee of the University of Utah.

For the mouse model of experimental metastasis, the mice were anesthetized with ketamine (100 mg/kg) and xylazine (13 mg/kg), the eye was proptosed, and 10^6 luciferase-expressing OMM2.5 cells in 100 μL of sterile PBS were injected into the retro-orbital sinus. Bioluminescence imaging of mice was performed weekly. Mice received an intraperitoneal injection of 150 μL of D-luciferin (Goldbio) for a dose of 150 mg/kg and were anesthetized

with isoflurane. Images were acquired using Perkin Elmer's In Vivo Imaging System Spectrum instrument.

Quantification was performed using Perkin Elmer Living Image software. Regions of interest boxes of identical size were used to calculate the total bioluminescence flux (photons/s) of the primary tumor and trunk metastases for each mouse at each time point. Outlier measurements (a >10-fold change compared to previous and subsequent weeks) were attributed to luciferin injection error and removed for final analysis. Images with significant bleeding of signal from the primary tumor were also excluded.

Survival and metastasis analyses

The TCGA UVM RNA-Seq dataset (n=80 patients) was downloaded using the GDCquery function in the TCGAbiolinks package in R. For uveal melanoma-specific survival analyses, only data for patients who died from uveal melanoma (n=76) were analyzed. For metastasis analyses, data for patients with time to metastasis information (n=70) were analyzed. Patients were divided on median expression into high- and low-expression groups. The survival and survminer packages were used to calculate univariate log-rank (Mantel-Cox) p-values and to plot survival curves with 95% confidence intervals in R. The Holm-Šídák procedure for multiple comparisons (i.e., multiple genes of interest) was used to adjust p-values.

Statistical analyses

GraphPad Prism (version 8.4) was used for all statistical tests except survival analyses. For all cellular assays, experiments were performed at least three times, and each plotted data point represents an experiment. When two unpaired groups were compared, unpaired t-tests were performed. Welch's correction was used when variance of the two groups was unequal. When three or more unpaired groups were compared, one-way ANOVA with Tukey's or Dunnett's multiple comparisons test was used. When the variances of the groups were unequal, the Welch's test and Dunnett's T3 test for multiple comparisons were used. For immunoblots, experimental conditions were normalized to the respective control for each replicate. Because these values are ratios, geometric means with 95% confidence intervals were plotted on a logarithmic scale. Two-tailed ratio paired t-tests or randomized block ANOVA with the Dunnett's or Holm-Šídák's test for multiple comparisons were performed to compute p-values. For studies involving measuring bioluminescence flux over time, the data were $\log_{10}$ transformed, and differences in the growth curves for the two conditions were statistically analyzed using a mixed effects model that employs a compound symmetry covariance matrix and is fit using restricted maximum likelihood. Significance at each time point was determined using the Šídák multiple comparison test.

Supplementary Material

Refer to Web version on PubMed Central for supplementary material.

ACKNOWLEDGMENTS

We thank D. Lim for graphics preparation. This research utilized both University of Utah and Huntsman Cancer Institute shared research resources including the Preclinical Research Resource, DNA Sequencing Core Facility, Bioinformatics Core Facility, and Fluorescence Microscopy Core Facility and was supported in part by the National Cancer Institute of the National Institutes of Health under Award Number P30CA042014. The content is solely the responsibility of the authors and does not necessarily represent the official views of the NIH.

FUNDING

This study was supported by the National Cancer Institute R00CA230312 (JHY), the Department of Defense Melanoma Research Program ME190288 (JHY), the Melanoma Research Foundation 51005681 (JHY), the National Institute of General Medical Sciences COBRE P20GM121316 (JHY), F30CA217184 (JRR), F30CA235964 (AT) and R01CA202778 (SJO).

DATA AVAILABILITY

All data that support the results of this study can be found within the main text and figures of this paper or in the Supplementary information.

REFERENCES

1. Damato EM, Damato BE. Detection and time to treatment of uveal melanoma in the United Kingdom: an evaluation of 2,384 patients. Ophthalmology 2012; 119: 1582–1589. [PubMed: 22503229]
2. Krantz BA, Dave N, Komatsubara KM, Marr BP, Carvajal RD. Uveal melanoma: epidemiology, etiology, and treatment of primary disease. Clin Ophthalmol 2017; 11: 279–289. [PubMed: 28203054]
3. Yavuzyigitoglu S, Koopmans AE, Verdijk RM, Vaarwater J, Eussen B, van Bodegom A et al. Uveal Melanomas with SF3B1 Mutations: A Distinct Subclass Associated with Late-Onset Metastases. Ophthalmology 2016; 123: 1118–1128. [PubMed: 26923342]
4. Grossniklaus HE. Understanding Uveal Melanoma Metastasis to the Liver: The Zimmerman Effect and the Zimmerman Hypothesis. Ophthalmology 2019; 126: 483–487. [PubMed: 30910033]
5. Khoja L, Atenafu EG, Suciu S, Leyvraz S, Sato T, Marshall E et al. Meta-analysis in metastatic uveal melanoma to determine progression free and overall survival benchmarks: an international rare cancers initiative (IRCI) ocular melanoma study. Ann Oncol 2019; 30: 1370–1380. [PubMed: 31150059]
6. Rowcroft A, Loveday BPT, Thomson BNJ, Banting S, Knowles B. Systematic review of liver directed therapy for uveal melanoma hepatic metastases. HPB (Oxford) 2020; 22: 497–505. [PubMed: 31791894]
7. Schank TE, Hassel JC. Immunotherapies for the Treatment of Uveal Melanoma-History and Future. Cancers (Basel) 2019; 11.
8. Piperno-Neumann S, Larkin J, Carvajal RD, Luke JJ, Schwartz GK, Hodi FS et al. Genomic Profiling of Metastatic Uveal Melanoma and Clinical Results of a Phase I Study of the Protein Kinase C Inhibitor AEB071. Mol Cancer Ther 2020; 19: 1031–1039. [PubMed: 32029634]
9. Falchook GS, Lewis KD, Infante JR, Gordon MS, Vogelzang NJ, DeMarini DJ et al. Activity of the oral MEK inhibitor trametinib in patients with advanced melanoma: a phase 1 dose-escalation trial. Lancet Oncol 2012; 13: 782–789. [PubMed: 22805292]
10. Carvajal RD, Piperno-Neumann S, Kapiteijn E, Chapman PB, Frank S, Joshua AM et al. Selumetinib in Combination With Dacarbazine in Patients With Metastatic Uveal Melanoma: A Phase III, Multicenter, Randomized Trial (SUMIT). J Clin Oncol 2018; 36: 1232–1239. [PubMed: 29528792]
11. Field MG, Durante MA, Anbunathan H, Cai LZ, Decatur CL, Bowcock AM et al. Punctuated evolution of canonical genomic aberrations in uveal melanoma. Nat Commun 2018; 9: 116. [PubMed: 29317634]

12. Shain AH, Bagger MM, Yu R, Chang D, Liu S, Vemula S et al. The genetic evolution of metastatic uveal melanoma. Nat Genet 2019; 51: 1123–1130. [PubMed: 31253977]
13. Rao PK, Barker C, Coit DG, Joseph RW, Materin M, Rengan R et al. NCCN Guidelines Insights: Uveal Melanoma, Version 1.2019. J Natl Compr Canc Netw 2020; 18: 120–131. [PubMed: 32023525]
14. Robertson AG, Shih J, Yau C, Gibb EA, Oba J, Mungall KL et al. Integrative Analysis Identifies Four Molecular and Clinical Subsets in Uveal Melanoma. Cancer Cell 2017; 32: 204–220 e215. [PubMed: 28810145]
15. Harbour JW, Onken MD, Roberson ED, Duan S, Cao L, Worley LA et al. Frequent mutation of BAP1 in metastasizing uveal melanomas. Science 2010; 330: 1410–1413. [PubMed: 21051595]
16. Worley LA, Onken MD, Person E, Robirds D, Branson J, Char DH et al. Transcriptomic versus chromosomal prognostic markers and clinical outcome in uveal melanoma. Clin Cancer Res 2007; 13: 1466–1471. [PubMed: 17332290]
17. Decatur CL, Ong E, Garg N, Anbunathan H, Bowcock AM, Field MG et al. Driver Mutations in Uveal Melanoma: Associations With Gene Expression Profile and Patient Outcomes. JAMA Ophthalmol 2016; 134: 728–733. [PubMed: 27123562]
18. Durante MA, Rodriguez DA, Kurtenbach S, Kuznetsov JN, Sanchez MI, Decatur CL et al. Single-cell analysis reveals new evolutionary complexity in uveal melanoma. Nat Commun 2020; 11: 496. [PubMed: 31980621]
19. Tanaka R, Terai M, Londin E, Sato T. The Role of HGF/MET Signaling in Metastatic Uveal Melanoma. Cancers (Basel) 2021; 13.
20. Oba J, Esmaeli B, Ellerhorst JA, Lyons GR, Milton DR, Wang WL et al. Trends in hepatocyte growth factor, insulin-like growth factor 1, thyroid-stimulating hormone, and leptin expression levels in uveal melanoma patient serum and tumor tissues: correlation to disease progression. Melanoma Res 2017; 27: 126–133. [PubMed: 28118269]
21. Yoshida M, Selvan S, McCue PA, DeAngelis T, Baserga R, Fujii A et al. Expression of insulin-like growth factor-1 receptor in metastatic uveal melanoma and implications for potential autocrine and paracrine tumor cell growth. Pigment Cell Melanoma Res 2014; 27: 297–308. [PubMed: 24354797]
22. Frenkel S, Zloto O, Pe'er J, Barak V. Insulin-like growth factor-1 as a predictive biomarker for metastatic uveal melanoma in humans. Invest Ophthalmol Vis Sci 2013; 54: 490–493. [PubMed: 23197685]
23. Yoo JH, Shi DS, Grossmann AH, Sorensen LK, Tong Z, Mleynek TM et al. ARF6 Is an Actionable Node that Orchestrates Oncogenic GNAQ Signaling in Uveal Melanoma. Cancer Cell 2016; 29: 889–904. [PubMed: 27265506]
24. Grossmann AH, Zhao H, Jenkins N, Zhu W, Richards JR, Yoo JH et al. The small GTPase ARF6 regulates protein trafficking to control cellular function during development and in disease. Small GTPases 2019; 10: 1–12. [PubMed: 28001501]
25. Hashimoto S, Onodera Y, Hashimoto A, Tanaka M, Hamaguchi M, Yamada A et al. Requirement for Arf6 in breast cancer invasive activities. Proc Natl Acad Sci U S A 2004; 101: 6647–6652. [PubMed: 15087504]
26. Palacios F, Price L, Schweitzer J, Collard JG, D'Souza-Schorey C. An essential role for ARF6-regulated membrane traffic in adherens junction turnover and epithelial cell migration. EMBO J 2001; 20: 4973–4986. [PubMed: 11532961]
27. Ratcliffe CDH, Siddiqui N, Coelho PP, Laterreur N, Cookey TN, Sonenberg N et al. HGF-induced migration depends on the PI(3,4,5)P3-binding microexon-spliced variant of the Arf6 exchange factor cytohesin-1. J Cell Biol 2019; 218: 285–298. [PubMed: 30404949]
28. Furman C, Short SM, Subramanian RR, Zetter BR, Roberts TM. DEF-1/ASAP1 is a GTPase-activating protein (GAP) for ARF1 that enhances cell motility through a GAP-dependent mechanism. J Biol Chem 2002; 277: 7962–7969. [PubMed: 11773070]
29. Sabe H, Hashimoto S, Morishige M, Ogawa E, Hashimoto A, Nam JM et al. The EGFR-GEP100-Arf6-AMAP1 signaling pathway specific to breast cancer invasion and metastasis. Traffic 2009; 10: 982–993. [PubMed: 19416474]

30. Laurent C, Valet F, Planque N, Silveri L, Maacha S, Anezo O et al. High PTP4A3 phosphatase expression correlates with metastatic risk in uveal melanoma patients. Cancer Res 2011; 71: 666–674. [PubMed: 21135111]
31. Ehlers JP, Worley L, Onken MD, Harbour JW. DDEF1 is located in an amplified region of chromosome 8q and is overexpressed in uveal melanoma. Clin Cancer Res 2005; 11: 3609–3613. [PubMed: 15897555]
32. Li R, Peng C, Zhang X, Wu Y, Pan S, Xiao Y. Roles of Arf6 in cancer cell invasion, metastasis and proliferation. Life Sci 2017; 182: 80–84. [PubMed: 28625359]
33. Perrin L, Belova E, Bayarmagnai B, Tuzel E, Gligorijevic B. Invadopodia enable cooperative invasion and metastasis of breast cancer cells. Commun Biol 2022; 5: 758. [PubMed: 35915226]
34. Onken MD, Worley LA, Ehlers JP, Harbour JW. Gene expression profiling in uveal melanoma reveals two molecular classes and predicts metastatic death. Cancer Res 2004; 64: 7205–7209. [PubMed: 15492234]
35. Onodera Y, Hashimoto S, Hashimoto A, Morishige M, Mazaki Y, Yamada A et al. Expression of AMAP1, an ArfGAP, provides novel targets to inhibit breast cancer invasive activities. EMBO J 2005; 24: 963–973. [PubMed: 15719014]
36. Muller MR, Rao A. NFAT, immunity and cancer: a transcription factor comes of age. Nat Rev Immunol 2010; 10: 645–656. [PubMed: 20725108]
37. Crabtree GR, Olson EN. NFAT signaling: choreographing the social lives of cells. Cell 2002; 109 Suppl: S67–79. [PubMed: 11983154]
38. Aramburu J, Yaffe MB, Lopez-Rodriguez C, Cantley LC, Hogan PG, Rao A. Affinity-driven peptide selection of an NFAT inhibitor more selective than cyclosporin A. Science 1999; 285: 2129–2133. [PubMed: 10497131]
39. Noguchi H, Matsushita M, Okitsu T, Moriwaki A, Tomizawa K, Kang S et al. A new cell-permeable peptide allows successful allogeneic islet transplantation in mice. Nat Med 2004; 10: 305–309. [PubMed: 14770176]
40. Collaborative Ocular Melanoma Study G. Assessment of metastatic disease status at death in 435 patients with large choroidal melanoma in the Collaborative Ocular Melanoma Study (COMS): COMS report no. 15. Arch Ophthalmol 2001; 119: 670–676. [PubMed: 11346394]
41. Valastyan S, Weinberg RA. Tumor metastasis: molecular insights and evolving paradigms. Cell 2011; 147: 275–292. [PubMed: 22000009]
42. Steeg PS. Targeting metastasis. Nat Rev Cancer 2016; 16: 201–218. [PubMed: 27009393]
43. Perotti V, Baldassari P, Bersani I, Molla A, Vegetti C, Tassi E et al. NFATc2 is a potential therapeutic target in human melanoma. J Invest Dermatol 2012; 132: 2652–2660. [PubMed: 22718120]
44. Shoshan E, Braeuer RR, Kamiya T, Mobley AK, Huang L, Vasquez ME et al. NFAT1 Directly Regulates IL8 and MMP3 to Promote Melanoma Tumor Growth and Metastasis. Cancer Res 2016; 76: 3145–3155. [PubMed: 27013197]
45. Qin JJ, Nag S, Wang W, Zhou J, Zhang WD, Wang H et al. NFAT as cancer target: mission possible? Biochim Biophys Acta 2014; 1846: 297–311. [PubMed: 25072963]
46. Grossmann AH, Yoo JH, Clancy J, Sorensen LK, Sedgwick A, Tong Z et al. The small GTPase ARF6 stimulates beta-catenin transcriptional activity during WNT5A-mediated melanoma invasion and metastasis. Sci Signal 2013; 6: ra14.
47. Gabriel CH, Gross F, Karl M, Stephanowitz H, Hennig AF, Weber M et al. Identification of Novel Nuclear Factor of Activated T Cell (NFAT)-associated Proteins in T Cells. J Biol Chem 2016; 291: 24172–24187. [PubMed: 27637333]
48. Britton S, Dernoncourt E, Delteil C, Froment C, Schiltz O, Salles B et al. DNA damage triggers SAF-A and RNA biogenesis factors exclusion from chromatin coupled to R-loops removal. Nucleic Acids Res 2014; 42: 9047–9062. [PubMed: 25030905]
49. Zhu W, London NR, Gibson CC, Davis CT, Tong Z, Sorensen LK et al. Interleukin receptor activates a MYD88-ARNO-ARF6 cascade to disrupt vascular stability. Nature 2012; 492: 252–255. [PubMed: 23143332]
50. Onken MD, Worley LA, Person E, Char DH, Bowcock AM, Harbour JW. Loss of heterozygosity of chromosome 3 detected with single nucleotide polymorphisms is superior to monosomy 3

for predicting metastasis in uveal melanoma. Clin Cancer Res 2007; 13: 2923–2927. [PubMed: 17504992]

51. Onken MD, Worley LA, Tuscan MD, Harbour JW. An accurate, clinically feasible multi-gene expression assay for predicting metastasis in uveal melanoma. J Mol Diagn 2010; 12: 461–468. [PubMed: 20413675]

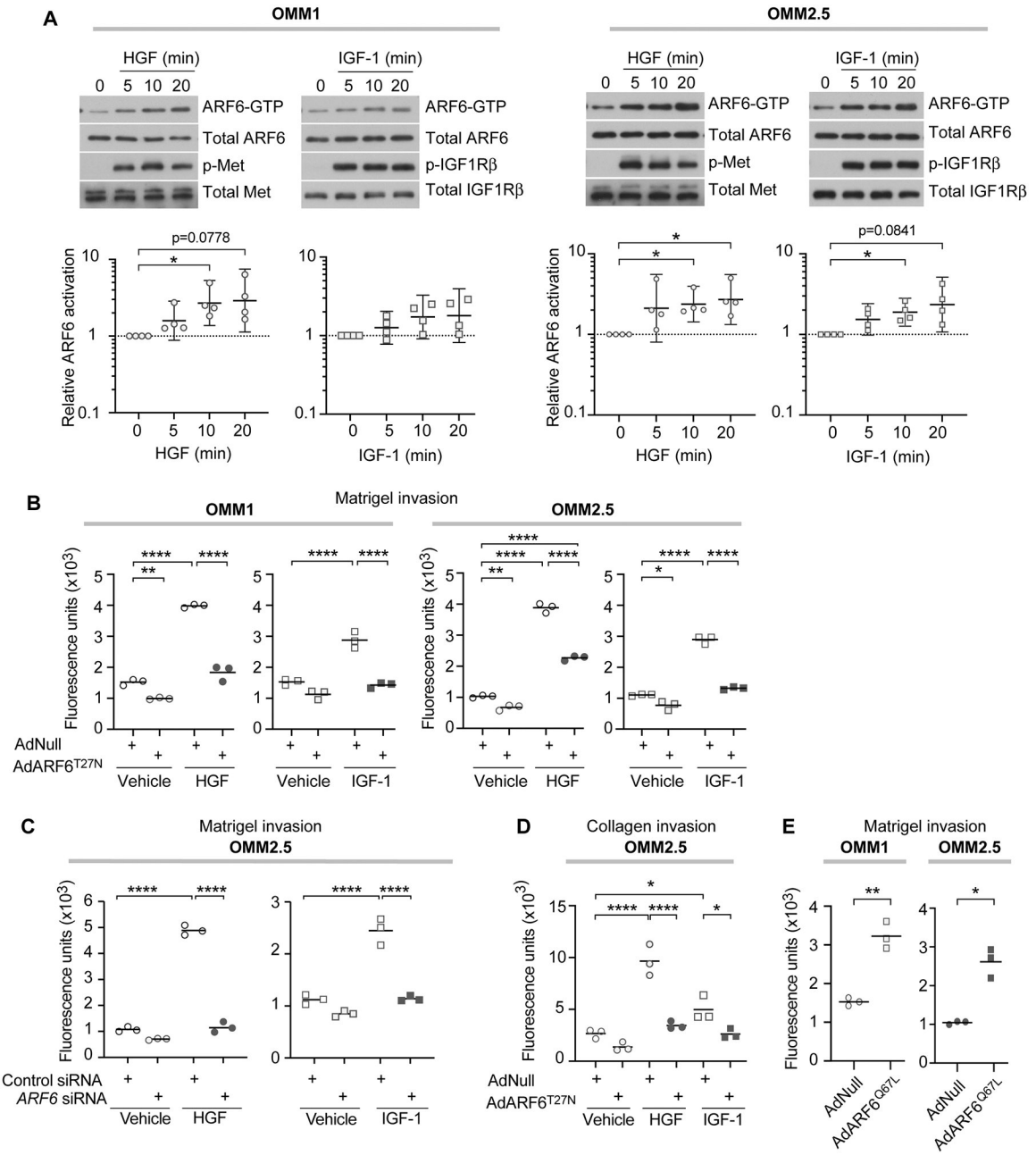

Fig. 1. ARF6 is hyperactivated by HGF and IGF-1 and promotes invasion of uveal melanoma cells.

A ARF6-GTP levels in OMM1 and OMM2.5 cells treated with HGF (50 ng/mL) or IGF-1 (100 ng/mL) for the indicated lengths of time. p-Met and p-IGF1Rβ are used for a positive control for treatment of HGF and IGF-1, respectively. ARF6 activation (normalized to time 0) is quantified in the graphs below the immunoblots. Data points from four experiments are displayed with the geometric means and 95% confidence intervals (CIs). p-values are corrected for multiple comparisons using Dunnett's multiple comparison test. **B** Invasion of OMM1 and OMM2.5 cells transduced with either a null (AdNull) or ARF6^{T27N} (Ad ARF6^{T27N}) adenovirus and treated with vehicle, HGF, or IGF-1. **C** Matrigel invasion of

HGF-, IGF-1-, or Vehicle-treated OMM2.5 cells in the presence of either Control siRNA or *ARF6* siRNA. **D** Collagen invasion of HGF-, IGF-1-, or Vehicle-treated OMM2.5 cells following transduction with either a AdNull or AdARF6^{T27N}. **E** Invasion of OMM1 and OMM2.5 cells transduced with either AdNull or AdARF6^{Q67L}. For B-E, data points from three independent experiments and the means are plotted. One-way ANOVA with Tukey's multiple comparisons test (B, C) or Šidák's multiple comparison test for selected comparisons (D); Two-tailed Welch's t test for (E). Only significant differences using a family-wise α=0.05 are indicated by asterisks. *p<0.05, **p<0.01, ****p<0.0001.

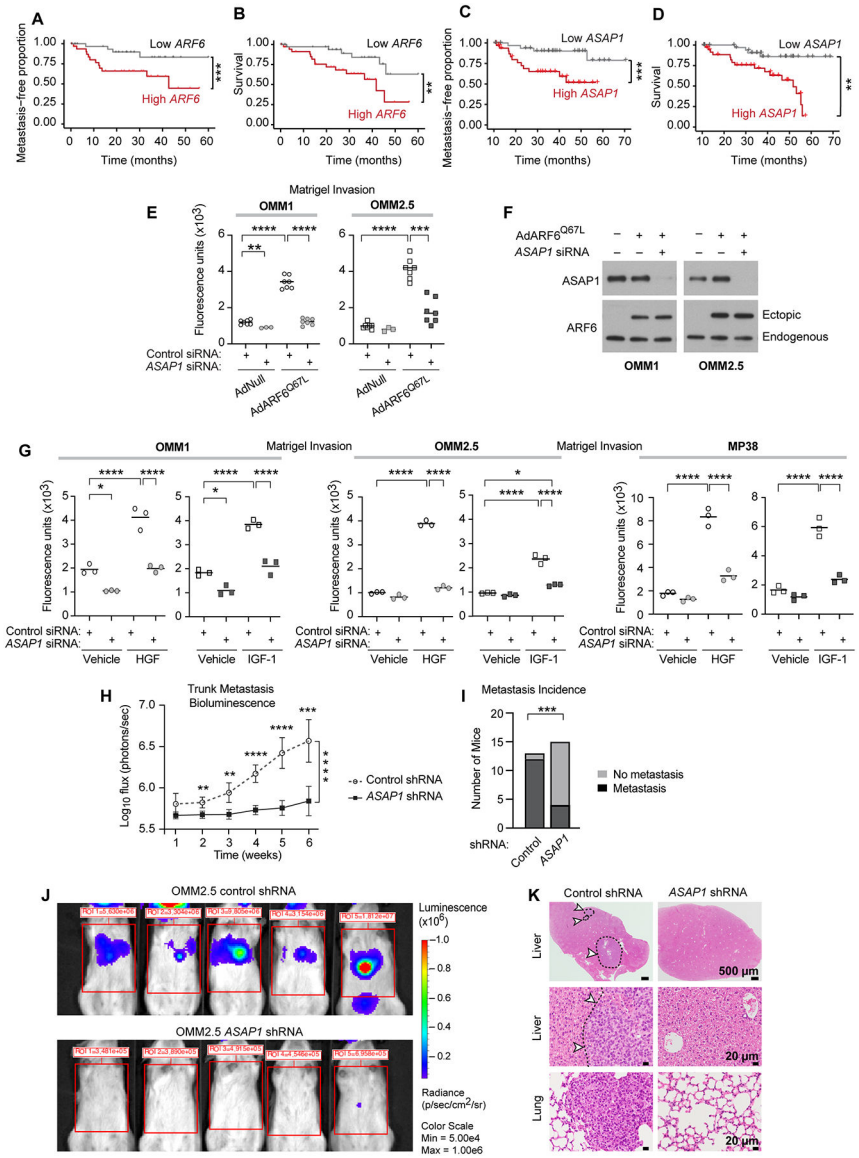

Fig. 2. ASAP1 is required for invasion and metastasis of uveal melanoma.

A, B, C, and **D** Kaplan-Meier plots for assessing the correlation between *ARF6* or *ASAP1* expression and uveal melanoma-specific metastasis (A and C; n=70) or survival (B and D; n=76) for patients in the TCGA UVM RNA-Seq dataset. Log-rank (Mantel-Cox) tests. **E** Invasion of OMM1 and OMM2.5 cells transduced with a null (AdNull) or ARF6^{Q67L} (AdARF6^{Q67L}) adenovirus and treated with control or *ASAP1* siRNA. Data points from three or seven independent experiments and means. One-way Welch's ANOVA with Dunnett's T3 multiple comparison test. **F** Immunoblots of lysates used in E to verify *ASAP1* knockdown and ectopic expression of ARF6^{Q67L}. **G** Matrigel invasion of OMM1, OMM2.5, and MP38 cells treated with control or *ASAP1* siRNA and vehicle, HGF, or IGF-1. Data points from three independent experiments and means. One-way ANOVA with Tukey's multiple comparisons test. **H** Bioluminescence flux in the abdomens of mice that received retro-orbital injections of OMM2.5 cells stably expressing either control (n=14)

or *ASAP1* (n=15) shRNA and luciferase. Means and 95% confidence intervals of $\log_{10}$-transformed data are displayed. Overall significance between the two groups was assessed with a mixed effects model that employs a compound symmetry covariance matrix and is fit using restricted maximum likelihood. Significance at each time point was determined using Šídák's multiple comparisons test. **I** Incidence of metastasis by bioluminescence imaging of mice in H at six weeks. Two-tailed Fisher's exact test. **J** Representative bioluminescence images of mice in H at six weeks. Region of interest windows used for quantification are displayed in red. **K** Representative H&E images from organs of mice in H at six weeks. Arrows indicate metastases. For all graphs, only significant differences using a family-wise α=0.05 are indicated with asterisks. *p<0.05, **p<0.01, ***p<0.001, ****p<0.0001.

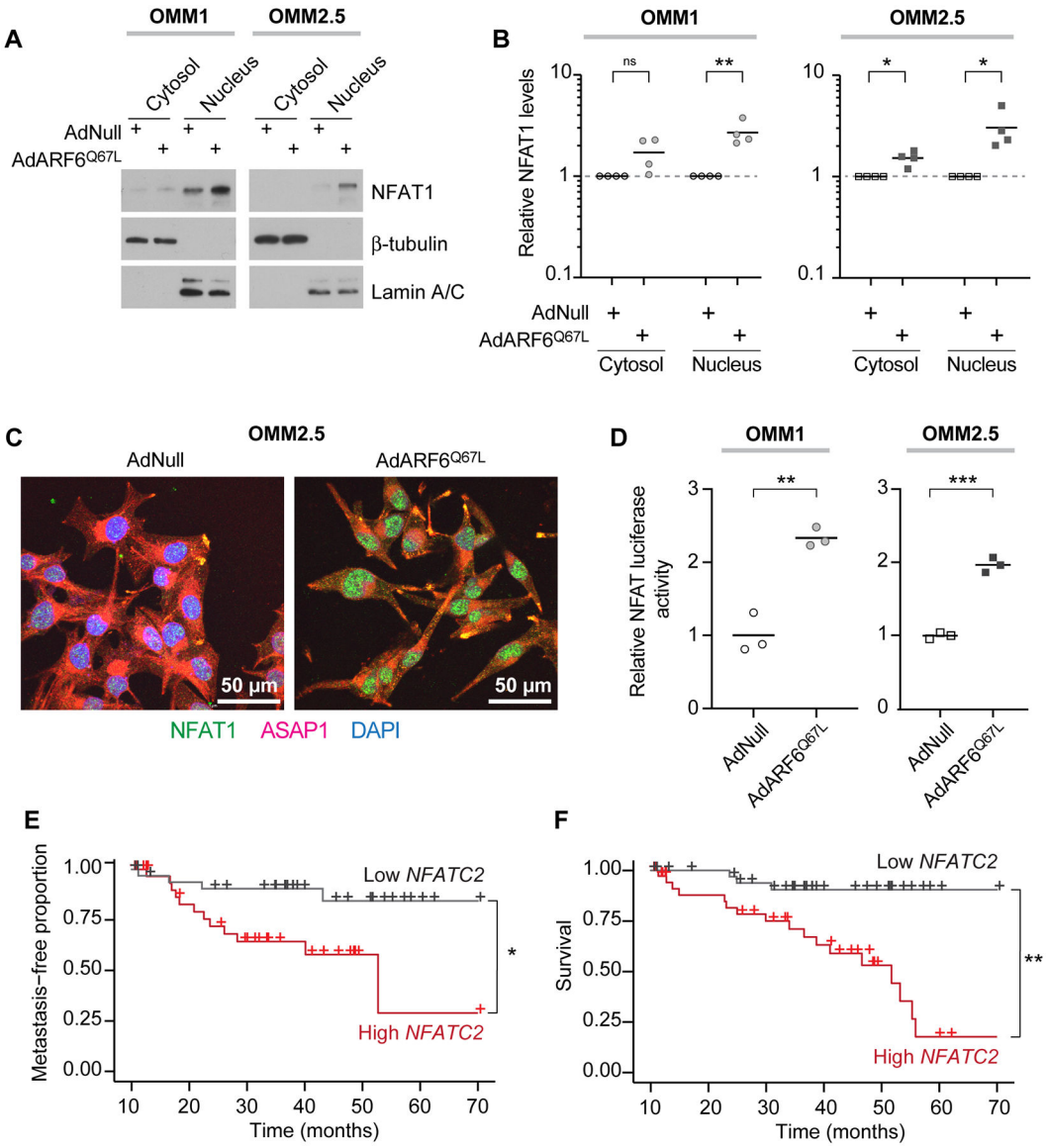

Fig. 3. Activated ARF6 increases NFAT1 nuclear localization and transcriptional activity.

A Subcellular fractionation of NFAT1 in OMM1 and OMM2.5 cells transduced with either a null (AdNull) or ARF6^{Q67L} (AdARF6^{Q67L}) adenovirus. β-tubulin is used as a positive control for the cytosolic fraction and Lamin A/C is used as a positive control for the nuclear fraction. **B** Quantification of subcellular NFAT1 levels shown in A (normalized to the AdNull control). Data points from four independent experiments are displayed with the geometric means and 95% confidence intervals (CIs). Two-tailed ratio paired t tests. **C** Immunocytofluorescence of NFAT1 (green) in OMM2.5 cells transduced with either a null (AdNull) or ARF6^{Q67L} (AdARF6^{Q67L}) adenovirus. Individual cells were visualized with ASAP1 (red) and DAPI (blue) staining. Scale bar, 50 µm. **D** NFAT transcriptional activity in OMM1 and OMM2.5 cells transduced with either a null (AdNull) or ARF6^{Q67L} (AdARF6^{Q67L}) adenovirus. Data points from three independent experiments with means. Unpaired two-tailed Student's t tests. **E** and **F** Kaplan-Meier plots for assessing the

correlation of *NFATC2* (*NFAT1*) expression and uveal melanoma-specific metastasis (E; n=70) and survival (F; n=76) for patients in the TCGA UVM RNA-Seq dataset. Log-rank (Mantel-Cox) tests. For all graphs, only significant differences at α=0.05 are indicated with asterisks. *p<0.05, **p<0.01, ***p<0.001.

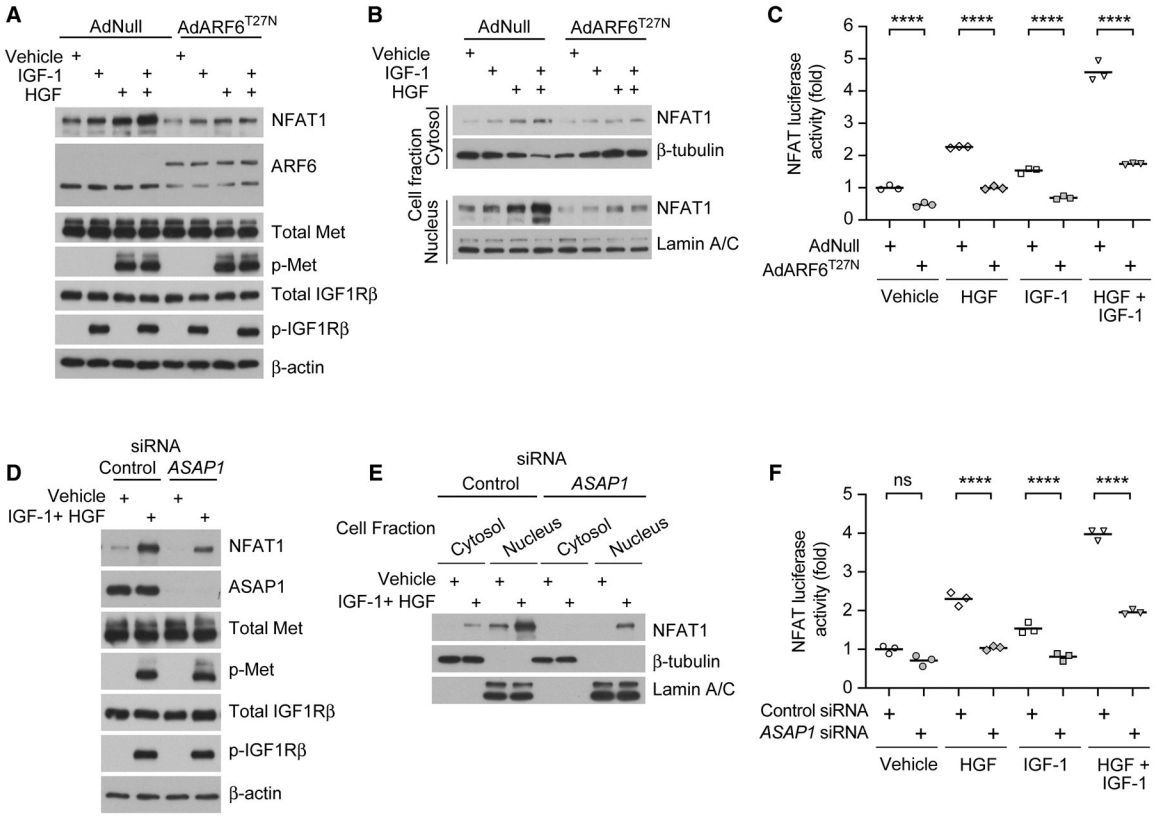

Fig. 4. Activated ARF6 and ASAP1 are required for both IGF-1 and HGF-induced NFAT1 nuclear localization and transcriptional activity.

A Total NFAT1 protein levels, **B** Subcellular fractionation, and **C** transcriptional activation of NFAT1 in OMM2.5 cells transduced with a null (AdNull) or ARF6^{T27N} (AdARF6 ^{T27N}) adenovirus and treated with vehicle, IGF-1 (100 ng/mL), HGF (50 ng/mL), or a combination of HGF and IGF-1. **D** Total NFAT1 protein levels, **E** Subcellular fractionation, and **F** transcriptional activation of NFAT1 in OMM2.5 cells treated with control or *ASAP1* siRNA and vehicle or the combination of IGF-1 (100 ng/mL) and HGF (50 ng/mL). For quantification of NFAT luciferase activity, data points and means from three independent experiments are plotted. One-way ANOVA with Tukey's multiple comparisons test. Only the most relevant comparisons are shown. **p<0.01, ****p<0.0001.

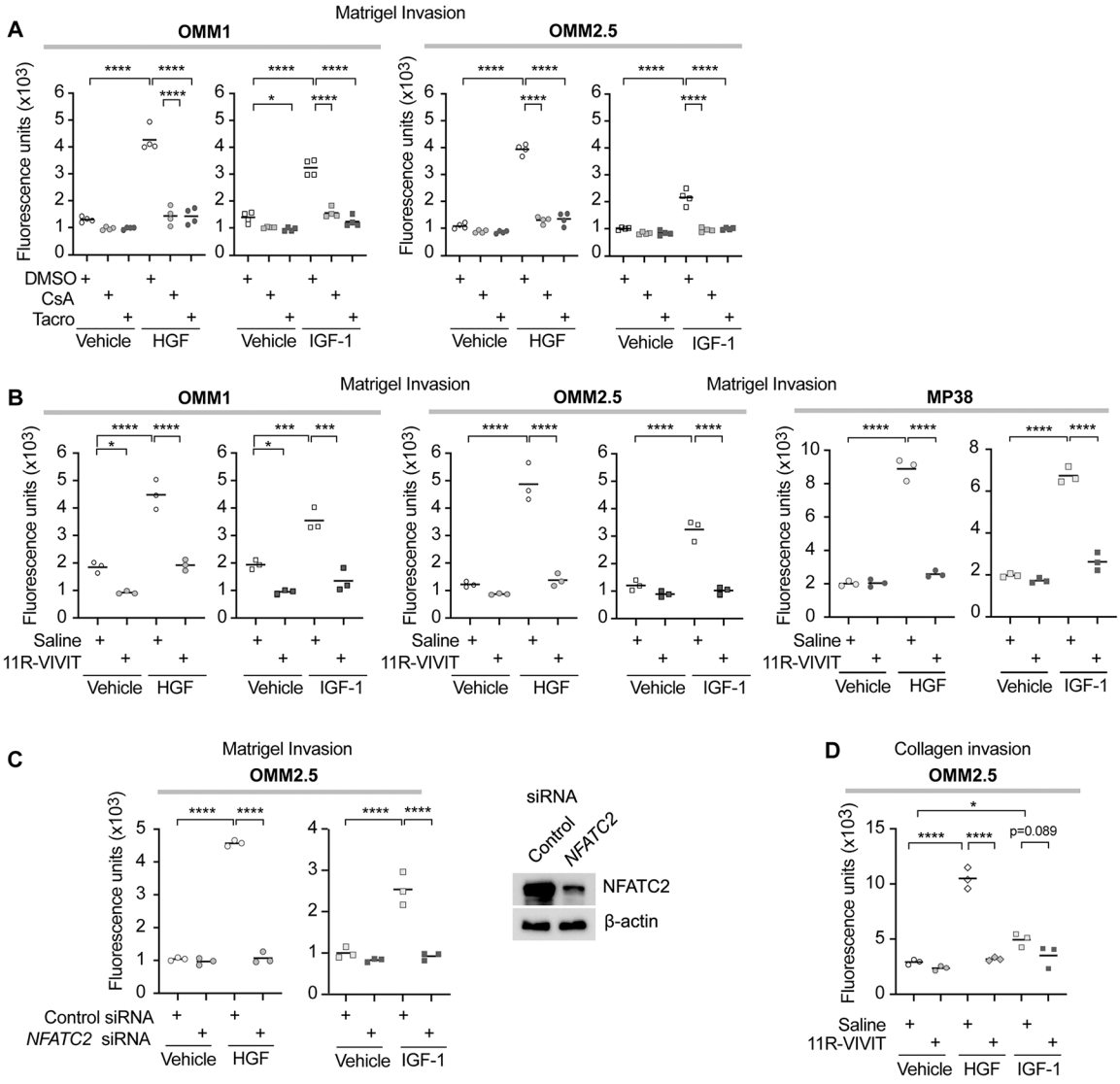

Fig. 5. Calcineurin and NFAT inhibitors reduce invasion of uveal melanoma cells.

A Invasion of OMM1 and OMM2.5 cells treated with DMSO, cyclosporin A (CsA; 1 μM), or tacrolimus (Tacro; 1 μM) and vehicle, HGF (50 ng/mL) or IGF-1 (100 ng/mL). **B** Matrigel invasion of OMM1, OMM2.5, and MP38 cells treated with saline or 11R-VIVIT (1μM) and vehicle, HGF (50 ng/mL) or IGF-1 (100 ng/mL). **C** Matrigel invasion of OMM2.5 cells treated with control or *NFATC2* siRNA and vehicle, HGF (50 ng/mL) or IGF-1 (100 ng/mL). Western blot showing the degree of *NFATC2* knockdown. **D** Collagen invasion of OMM2.5 cells treated with saline or 11R-VIVIT (1μM) and vehicle, HGF (50 ng/mL) or IGF-1 (100 ng/mL). Data points from three or four independent experiments and their means. One-way ANOVA with Tukey's multiple comparisons test (A-C) or Šidák's multiple comparison test for selected comparisons (D). Only the most relevant comparisons are shown. *p<0.05, ***p<0.001, ****p<0.0001.

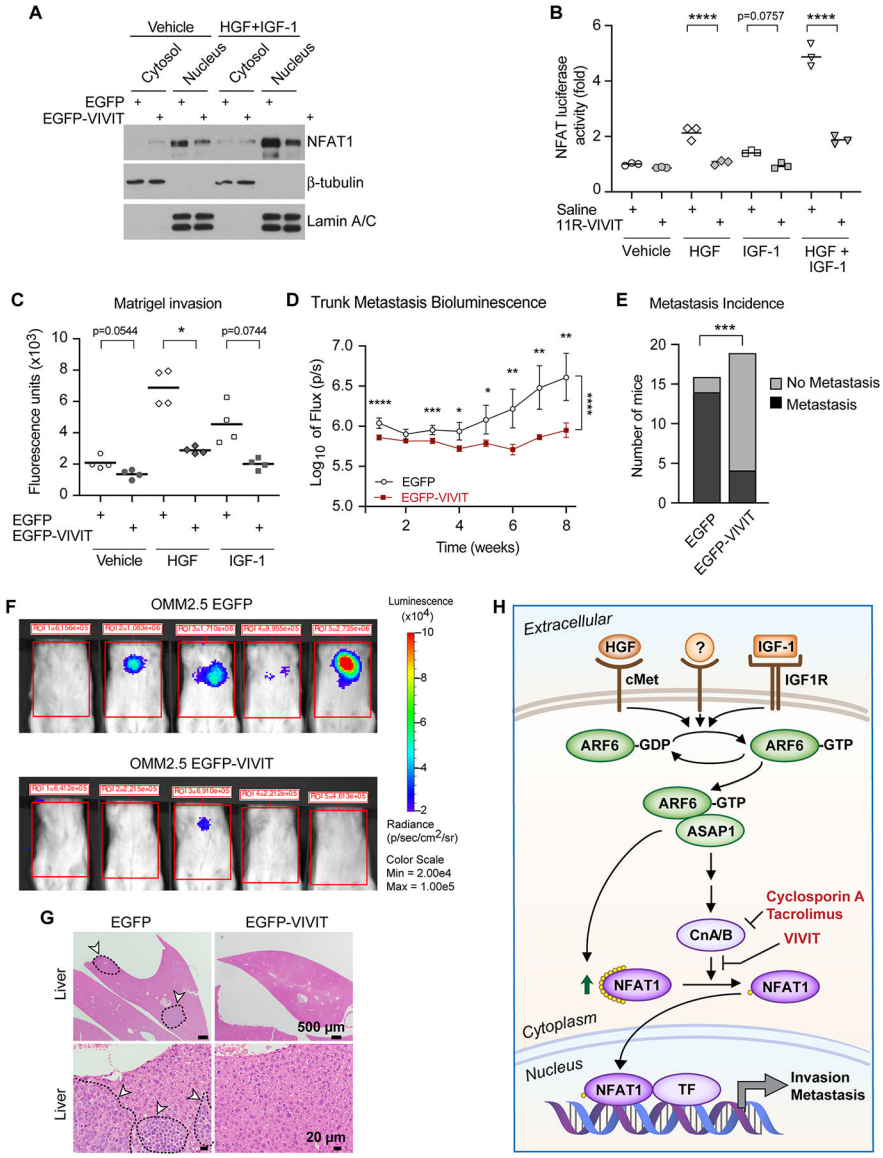

Fig. 6. Inhibition of NFAT reduces metastasis *in vivo*.

A Subcellular fractionation of NFAT1 from OMM2.5 cells stably expressing either EGFP or EGFP-VIVIT treated with vehicle or the combination of HGF (50 ng/mL) and IGF-1 (100 ng/mL). β-tubulin immunoblot is used as a positive control for cytosolic fraction and Lamin A/C immunoblot is used as a positive control for nuclear fraction. **B** NFAT transcriptional activity in OMM2.5 cells treated with saline or 11R-VIVIT and vehicle, HGF (50 ng/mL), IGF-1 (100 ng/mL, or a combination of HGF and IGF-1. Data from three independent experiments with means. One-way ANOVA and Tukey's multiple comparisons test showing relevant comparisons. **C** Invasion of OMM2.5 cells stably expressing EGFP or EGFP-VIVIT treated with vehicle, HGF (50 ng/mL), or IGF-1 (100 ng/mL). Data from four independent experiments are plotted along with the means. The p values for relevant comparisons using Welch's one-way ANOVA with Dunnett's T3 multiple comparisons test. **D** Bioluminescence flux in the abdomens of mice that received retro-orbital injections of

OMM2.5 cells stably expressing either EGFP (n=20) or EGFP-VIVIT (n=20). Arithmetic means and 95% confidence intervals are displayed for $\log_{10}$-transformed data. Overall significance between the two groups was assessed with a mixed effects model that employs a compound symmetry covariance matrix and is fit using restricted maximum likelihood. Significance at each time point was determined using Holm-Šídák's multiple comparisons test. **E** Incidence of metastasis by bioluminescence imaging of mice in C at eight weeks. Two-tailed Fisher's exact test. **F** Representative bioluminescence images of abdomens of mice in C at eight weeks. **G** Representative H&E images from livers of mice in C at eight weeks. Arrows point to metastases. For all plots, *p<0.05, **p<0.01, ***p<0.001, ****p<0.0001. Only significant results (α=0.05) are indicated, except in panel B where actual p values are given for a few comparisons that did not reach statistical significance. **H** Proposed HGF–IGF-1–ARF6–ASAP1–NFAT1 signaling pathway that controls invasion and metastasis of uveal melanoma.